Molecular Catalysis 553 (2024) 113718

Contents lists available at ScienceDirect

Molecular Catalysis

journal homepage: www.journals.elsevier.com/molecular-catalysis

Sorption-enhanced glycerol steam reforming over lithium cuprate-based bifunctional material for the production of high-purity hydrogen

Prabijna S.S. Babu [a,b], Prakash D. Vaidya [a,*]

[a] Department of Chemical Engineering, Institute of Chemical Technology, Matunga (East), Mumbai 400 019, India
[b] Department of Chemistry, Ramniranjan Jhunjhunwala College, Ghatkopar (West), Mumbai 400 086, India

ARTICLE INFO

Keywords:
Lithium cuprate
Hydrogen production
Sorption-enhanced
Glycerol steam reforming
Carbon dioxide adsorption

ABSTRACT

We investigated the production of high-purity H_2 through sorption-enhanced glycerol steam reforming (SEGSR) using lab-made bifunctional materials consisting of nickel, Al_2O_3, and Li_2CuO_2. Different bifunctional materials were prepared with 10 wt % Ni loading but varying wt % of Al_2O_3 and Li_2CuO_2, and their catalytic activity was evaluated in a continuous fixed-bed down-flow reactor. HM-50, which had an equal wt % of Al_2O_3 and Li_2CuO_2, showed the highest performance. The conversion of glycerol and the purity of H_2 were examined with respect to temperature, feed flow rate, and steam-to-carbon molar ratio (S/C). At the optimum reaction conditions (temperature = 700 °C, feed flow rate = 0.5 ml/min, and S/C = 6), glycerol conversion and H_2 purity were 100 % and 94 mol %, respectively. The adsorption capacity of HM-50 was found to be 3.9 mmol CO_2 per gram. With a breakthrough time of 15 min, the substance was stable for 13 adsorption-desorption cycles. The material was regenerated by substituting the feed with a N_2 and steam mixture heated to 700 °C for 30 min. A most likely reaction mechanism suggested that glycerol was catalytically converted to acetaldehyde, which was then quickly decomposed to CO and CH_4. We are the first research team to investigate the use of Li_2CuO_2 in any steam reforming process.

1. Introduction

On 15th August 2021, India announced its National Hydrogen Mission (NHM), with the goal of achieving energy independence by the year 2047 and net zero emissions by the year 2070 [1]. By using more energy generated from renewable resources, this objective can be met. The transition to clean energy is thought to be well on its way with hydrogen, a new-age fuel [2]. Currently, about 95 % of H_2 is produced from fossil-fuel-based raw materials, 4 % from the electrolysis of water, and 1 % from biomass-based sources [3]. Commercially it is produced by conventional steam methane reforming (SMR) [4–6]. Since CH_4 comes from fossil fuels, it is not a renewable feed for H_2 production. However, biomass or feedstocks produced from biomass must be employed for the sustainable generation of H_2 [3,7,8]. This path is environmentally friendly because it produces no carbon. One such sustainable feedstock is glycerol ($CH_2OH—CHOH—CH_2OH$ or $C_3H_8O_3$), a byproduct of the manufacturing of biodiesel. Through steam reforming, over an appropriate catalyst, it can be converted to H_2 [9,10]. The unappealing crude glycerol is valorized by glycerol steam reforming (GSR) [11]. Moreover, glycerol has attracted the interest of a substantial number of researchers for H_2 production in the past 10 years [12–18] due to its wide availability, low cost, and high hydrogen concentration.

Although GSR involves several equilibrium reactions, the overall reaction, represented by Eq. (1), indicates that theoretically 7 mol of H_2 can be produced per mole of glycerol converted via a steam reforming process [10,19]. However, the occurrence of the side reactions decreases the yield and purity of H_2 [10]. This reaction is a combination of the glycerol decomposition (the main reaction), Eq. (2), and the water gas shift (WGS) reaction (a side reaction), Eq. (3). These reactions are carried out in separate reactors due to the endothermic and exothermic nature of them. Other side reactions like CO methanation, Eq. (4); CO_2 methanation, Eq. (5); SMR, Eq. (6), and many more like Eqs. (7) and (8) may occur too. Eqs. (6) and (8) are reverses of Eqs. (4) and (3), respectively [9–11]. Due to the equilibrium nature of the reaction, Eq. (1) can only produce H_2 with a maximum purity of about 70 mol % in the exit gas stream [11,19]. Therefore, CO_2 separation is done downstream to produce high-purity (> 90 mol %) H_2. This makes the GSR process more complex and raises the price of H_2 produced by this technique.

* Corresponding author.
E-mail address: pd.vaidya@ictmumbai.edu.in (P.D. Vaidya).

https://doi.org/10.1016/j.mcat.2023.113718
Received 1 August 2023; Received in revised form 20 November 2023; Accepted 21 November 2023
Available online 12 December 2023

Overall GSR reaction: $C_3H_8O_3 + 3H_2O \rightleftharpoons 3CO_2 + 7H_2$, $\Delta H^{\circ}_{298K} = +128$ kJ mol^{-1} (1)

Glycerol decomposition: $C_3H_8O_3 \rightleftharpoons 3CO + 4H_2$, $\Delta H^{\circ}_{298K} = +251$ kJ mol^{-1} (2)

Water gas shift (WGS) reaction: $3CO + 3H_2O \rightleftharpoons 3CO_2 + 3H_2$, $\Delta H^{\circ}_{298K} = -41$ kJ mol^{-1} (3)

CO-methanation: $CO + 3H_2 \rightleftharpoons CH_4 + H_2O$, $\Delta H^{\circ}_{298K} = -206$ kJ mol^{-1} (4)

CO_2-methanation: $CO_2 + 4H_2 \rightleftharpoons CH_4 + 2H_2O$, $\Delta H^{\circ}_{298K} = -165$ kJ mol^{-1} (5)

Steam methane reforming (SMR): $CH_4 + H_2O \rightleftharpoons CO + 3H_2$, $\Delta H^{\circ}_{298K} = +206$ kJ mol^{-1} (6)

Dry methane reforming (DMR): $CH_4 + CO_2 \rightleftharpoons 2CO + 2H_2$, $\Delta H^{\circ}_{298K} = +247$ kJ mol^{-1} (7)

Reverse water gas shift (RWGS): $H_2 + CO_2 \rightleftharpoons CO + H_2O$, $\Delta H^{\circ}_{298K} = +41$ kJ mol^{-1} (8)

The sorption-enhanced glycerol steam reforming (SEGSR) process [19–21], which combines H_2 production (GSR) and H_2 purification (CO_2 adsorption) in a single reactor, overcomes the equilibrium limitations of GSR. It uses a reforming catalyst and a CO_2 - selective sorbent to produce high-purity H_2. According to the well-known Le Chatelier's principle of chemistry [11,21], when CO_2 is removed in situ by the sorbent, the equilibrium is shifted in favor of the generation of H_2, Eq. (1). As a result, the product gas stream only comprises H_2 (and no CO_2) until the entire amount of CO_2 produced during the reaction is adsorbed by the sorbent that has been deployed in the reactor. Thus, SEGSR lowers the operating temperature by balancing the energy from the exothermic carbonation reaction, simplifies the reaction by omitting the need for downstream processing, and lowers the cost of producing high-purity H_2 [10,15,21]. However, an effective reforming catalyst and an appropriate CO_2 sorbent are required for SEGSR to produce high-purity H_2 successfully.

Fast adsorption and desorption kinetics, high adsorption capacity, sufficient mechanical strength, and improved multi-cycle stability are all desirable characteristics of a CO_2 sorbent [22–25]. For sorption-enhanced steam reforming (SESR) processes, three general groups of CO_2-sorbents—CaO-based [24,26], hydrotalcite (Htlc)-based [22,27], and alkali metal ceramics [22–24]—are used. The CaO-based materials have extremely poor multi-cycle stability [26,28], quick sorption kinetics, and a remarkable capacity to collect CO_2. Hydrotalcites (layered double hydroxides) exhibit low adsorption capacity but moderate sorption kinetics and acceptable multi-cycle stability [29,30]. Alkali metal ceramics are binary metal oxides that contain at least one element from Group I (alkali metal) of the modern periodic table [23]. They have all the qualities necessary to be a reliable CO_2-selective sorbent, including a large carbonation temperature window. At low CO_2 partial pressures, however, their adsorption kinetics considerably slows down [23,24]. Alkali metal ceramics for SERP have been extensively studied, including lithium orthosilicate (Li_4SiO_4) [31,32], lithium zirconate (Li_2ZrO_3) [21,33,34], and sodium zirconate (Na_2ZrO_3) [35,36]. Lithium ferrite ($LiFeO_2$) [24], lithium cuprate (Li_2CuO_2) [37,38], and potassium sodium titanate ($KNaTiO_3$) [39] are other alkali metal ceramics that have exceptional sorption capabilities but have not yet been investigated for SERP. We were the first research team to assess $KNaTiO_3$'s effectiveness for SERP [39].

Among all the reported alkali metal ceramics, Li_2CuO_2 demonstrates exceptional CO_2 chemisorption capabilities [37]. 9.14 mmol CO_2/g is its highest adsorption capacity. It displays surface-level chemisorption between 120 and 500 °C and then bulk chemisorption up to 700 °C. The range of its desorption temperature is 700–840 °C. Additionally, lithium sublimation causes its breakdown above 840 °C [37]. Eq. (9) represents its carbonation reaction.

Li_2CuO_2 (s) + CO_2 (g) ⇌ CuO (s) + Li_2CO_3 (s) (9)

The process of carbonation (adsorption) produces CuO and Li_2CO_3. But during regeneration (calcination), which is accomplished by flowing a mixture of N_2 and steam for 20 to 30 min at the reaction temperature itself, the opposite reaction takes place. It has noticeable adsorption properties even at low CO_2 partial pressures, in contrast to other alkali metal ceramics [40]. The CO_2 adsorption process is stabilized by the presence of nickel [40], whilst the water vapor helps both the adsorption and desorption processes [41].

The noble metal-based catalysts (Pd, Pt, Ru, and Rh) are the favored option for SEGSR due to their superior reforming activity and increased resistance to coke formation. However, their expensive price prevents them from being commercialized [11,15]. In order to catalyze the steam reforming processes, low-cost materials based on Co or Ni are being increasingly used [9,11,15,18,42]. The coke deposition makes them relatively more vulnerable to deactivation, which can be reduced by utilizing appropriate support and promoter. Alumina (Al_2O_3) has grown to be the most popular catalyst support due to its large surface area and outstanding thermal stability [18,21].

Today, a single substance called a hybrid material, made up of both the catalyst and the sorbent, is being produced and employed [15,28,43] rather than loading a reactor with two different materials (the reforming catalyst and the sorbent). A hybrid material, also known as a bifunctional material, functions both as a sorbent and a catalyst at the same time. By removing the barriers posed by diffusion, these materials provide quicker and better access to the catalytic and sorption sites, thereby improving the yield and purity of H_2 [22,28].

The present work examined the production of high-purity H_2 via SEGSR over lab-made new hybrid materials (Ni/Al_2O_3/Li_2CuO_2) that contained varied amounts of Al_2O_3 and Li_2CuO_2 but loading of 10 wt % Ni. The best-performing bifunctional material was used for the determination of the optimal process conditions needed to generate high-purity H_2. Additionally evaluated were the best performer's sorption capability and multi-cycle stability. A most likely reaction mechanism for the SEGSR was also proposed. We are the first research team to examine the use of Li_2CuO_2 for any steam reforming method, as far as our search of the literature is concerned. The study's findings agree with the information available in the literature.

2. Experimental

2.1. Materials

All necessary chemicals were acquired from S.D. Fine-Chem Limited, Mumbai, India. We bought N_2, H_2, and CH_4 gas cylinders as well as calibration gas mixture canisters, from Rakhangi Gas Services, Mumbai, India.

2.2. Synthesis of lithium cuprate (Li_2CuO_2)

A solid-state reaction between Li_2CO_3 and CuO produced Li_2CuO_2. These precursors were combined in the proper amounts and pounded into a fine powder in an agate mortar for one hour while having 20 wt percent extra lithium present to account for its sublimation. It was then calcined at 800 °C for 6 h in air, cooled, and ground into a fine powder [40].

2.3. Synthesis of hybrid materials

The materials Ni/Al_2O_3, Ni/Li_2CuO_2, and Ni/Al_2O_3/Li_2CuO_2 were synthesized by the wet impregnation method [39,43]. This method involved adding a solution of nickel nitrate drop by drop to a calculated amount of Al_2O_3 and/or Li_2CuO_2 powder while continuously stirring. The resulting mixture was stirred at room temperature for 5 h before the temperature was raised to 80 °C and stirring continued until a solid mass formed. In an oven, it was dried for the entire night at 110 °C and then calcined at 700 °C for 4 h in air to obtain the desired product. The

calcined material was crushed and sieved to obtain particles with a mesh size of 30 – 60. All the materials had 10 wt % nickel loading. The designation HM was given to Ni/Li_2CuO_2, while $Ni/Al_2O_3/Li_2CuO_2$ was labeled as HM-20, HM-50, or HM-80 depending on whether it contained 20:80, 50:50, or 80:20 wt % ratio of Li_2CuO_2:Al_2O_3.

2.4. Characterization of the materials

To analyze the materials, various techniques were used including X-ray diffraction (XRD), scanning electron microscope (SEM), energy dispersive X-ray spectrometer (EDX), Brunauer-Emmett-Teller (BET) method, Barett-Joyner-Halenda (BJH) method, H_2-pulse chemisorption, H_2-temperature programmed reduction (TPR), and CO_2-temperature programmed desorption (TPD). XRD spectra were obtained through a Rigaku-mini flex powder diffractometer using a Cu target K_α radiation of wavelength 1.54 Å. The diffraction patterns were recorded by scanning 2θ range from 10° to 80°. SEM-EDX data were collected using a JEOL-JSM6380 LA instrument to determine the morphology and elemental composition of the material. AXIS Supra, Kratos Analytical (UK) instrument was used to record X-ray photoelectron spectroscopic (XPS) data. Monochromatic Al K-alpha was the X-ray source for the XPS analysis. The N_2 adsorption-desorption experiments were conducted using a QuantaChrome Nova 2200e Surface Area & Pore Size Analyzer instrument. The BET equation was utilized to determine the specific surface area and the BJH method was used to estimate the pore properties of the materials. Sample degassing was performed at 120 °C for 12 h before testing. To assess the reducibility of the bifunctional material, a TPR profile was obtained using a Microtrac BELCAT II instrument. About 100 mg of unreduced material was heated in a U-shaped tube at a rate of 10 °C min^{-1} to 700 °C, under a flow rate of 30 ml min^{-1} of 10 vol % H_2-Ar. The thermal conductivity detector (TCD) signals were continuously recorded to determine the consumption of H_2. Additionally, an H_2-pulse chemisorption analysis was conducted on the same instrument to determine the dispersion of the active metal (nickel). Similarly, a TPD study was carried out on a Micromeritics AutoChem II 2920 instrument, using approximately 100 mg of unreduced sample. The sample was pretreated with helium at 800 °C for 30 min, then cooled to 50 °C. The probe gas (10 % CO_2-He) was injected through the sample bed until saturation, which was monitored from the TCD signals. The excess probe gas was flushed out with He as a carrier gas. Finally, the desorption study was performed by increasing the temperature to 800 °C at a heating rate of 20 °C min^{-1} using 30 ml min^{-1} He as a carrier gas. To calibrate the TCD, 10 vol % CO_2—He was used.

2.5. Experimental setup

A 50 cm long, 19 mm inner diameter and 25.4 mm outer diameter SS-316 tubular down-flow fixed-bed reactor was used for all reactions. An enclosed furnace heated the reactor to the desired temperature. The control panel managed the temperature, pressure, and gas flow. A gas chromatograph (GC) equipped with a TCD and a HayeSep DB column was also part of the system, along with feed tanks, HPLC pumps, vaporizers, a premix heater, and a weighing scale.

2.6. Steam reforming of glycerol

The reactor was loaded with a weighed quantity of powdered material (up to 3 g) by sandwiching it between two beds of quartz wool. Under the N_2 flowing rate of 40 ml/min, the reactor was heated to the desired temperature. In each reaction, N_2 was utilized as a carrier gas. The loaded material was reduced for two hours at 515 °C with a gas flow rate of 10 ml/min H_2 + 40 ml/min N_2 prior to beginning a reforming reaction. After that, N_2 was passed through the reactor at a rate of 100 ml/min to flush H_2 out of it. Monitoring the TCD signals in the GC allowed us to confirm that there was no H_2 in the outlet gas stream. A vaporizer (kept at 250 °C) was fed an aqueous solution of glycerol at the required flow rate by an HPLC pump. Through a premix heater that was kept at 300 °C, the vaporized feed was transported to the reactor. The system's pressure was kept constant at 1 bar. The inline GC was used to analyze the outflow stream from the reactor after it had been progressively passed through two water condensers, a gas-liquid separator, and a moisture trap. A 5-minute time limit was specified for each GC run for a gas sample. The TCD picked up gases like H_2, CO, CH_4, and CO_2. The calibration curves for the individual gases were used to calculate the concentration of the gases in the outlet gas stream. By injecting gas mixtures with precisely defined compositions (procured in 8–10 canisters) in GC under the set conditions, the calibration curves were obtained. Similarly, every 15 min, the liquid samples were taken and analyzed in a different GC fitted with a Tenax column and a flame ionization detector (FID). A liquid sample run had a 20 min time limit. For all GC analyses, H_2 and N_2 gases were employed as the flame gas and the carrier gas, respectively. By injecting the pure as well as standard solutions of the anticipated liquid components, calibration curves were created for liquid samples.

2.7. Test for metal ion leaching

Liquid samples were collected after every 30 min of the reaction and examined for the presence of Ni^{2+}, Cu^{2+}, and Al^{3+} ions to determine if metal ion leaching had taken place or not. For each test, a liquid sample of 1–2 cm^3 was used. When bubbling H_2S gas through an acidic medium, the absence of black precipitate indicated that there was no Cu^{2+} present in the test solution. The lack of a reddish-brown precipitate when potassium hexacyanoferrate (II) solution was added to the acidified portion of the liquid sample further supported the absence of Cu^{2+}. Similarly, the absence of Ni^{2+} was confirmed by the lack of a scarlet red precipitate using the dimethyl glyoxime reagent in an ammoniacal solution. When a test portion of the liquid sample was treated with the quinalizarin reagent, no red precipitate formed, which is a sign that Al^{3+} isn't present [44]. All of the expected ions were found to be absent from the tests. Therefore, there was no metal ion leaching during the reaction.

2.8. Mathematical expressions

The mathematical expressions used for the calculation of various reaction parameters are given in Eqs. (10) – (14).

$$\text{Gas hourly space velocity (GHSV)} = \text{inlet gas flow rate in } ml\ min^{-1} / \text{w} \quad (10)$$

where w is the gram of the solid material loaded into the reactor.

$$\text{Glycerol conversion (\%)} = 100 \times \{[\text{Glycerol}]_{in} - [\text{Glycerol}]_{out}\} / [\text{Glycerol}]_{in} \quad (11)$$

where, $[\text{Glycerol}]_{in}$ and $[\text{Glycerol}]_{out}$ are the inlet and outlet flow rates of glycerol in mol/h.

$$H_2 \text{ yield (\%)} = 100 \times [H_2]_{out} / \{7 \times [\text{Glycerol}]_{converted}\} \quad (12)$$

where, $[\text{Glycerol}]_{converted} = [\text{Glycerol}]_{in} - [\text{Glycerol}]_{out}$

$$H_2 \text{ mol \%} = 100 \times [H_2]_{out} / \text{total outlet gas flow rate in mol/h;} \quad (13)$$

where $[H_2]_{out}$ is the outlet flow rate of hydrogen in mol/h.

Eq. (12) gives the amount of hydrogen produced during the reaction and Eq. (13) tells how pure the produced H_2 is.

The adsorption capacity (Q_{ads}) of a material is given by:

$$Q_{ads} = F.\ C_o.\ t_b / w \quad (14)$$

where F is the total flow rate of the feed gas in *mol/min*; C_o and t_b are the *mole fraction* of CO_2 and the time in minutes, respectively, at which CO_2 is first detected in the product gas stream during a steam reforming reaction. In a fixed-bed column, the loaded material's working CO_2 adsorption capacity under dynamic conditions is calculated by

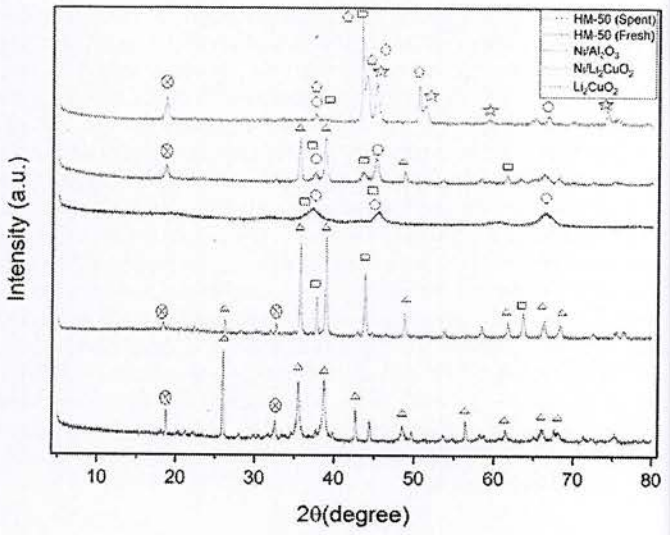

Fig. 1. XRD patterns of Li_2CuO_2, Ni/Li_2CuO_2, Ni/Al_2O_3, HM-50 (fresh) and HM-50 (spent). △= Li_2CuO_2, □ = NiO, ☆ = CuO, ⬠ = Li_2CO_3 and ○ = Al_2O_3, and ⊗ = Li_2O.

Table 1
The average crystallite size (nm) of various phases (calculated from the XRD peaks by the Scherrer equation).

Catalyst	NiO	Li_2CuO_2	CuO	Li_2CO_3
Ni/Al_2O_3 [a]	Could not be determined due to overly broad peaks	—	—	—
Ni/Li_2CuO_2 [a]	28	33	—	—
HM-50 (fresh)[a]	16	32	—	—
HM-50 (spent)[b]	28	—	29	19

[a] unreduced & before SEGSR.
[b] after 18 adsorption-desorption cycles.

Table 2
BET surface area and pore properties of the synthesized materials.

Samples	N_2-BET surface area (m^2/g)	Total pore volume (cm^3/g)	Average pore diameter (nm)
Li_2CuO_2 [a]	4.7	0.017	3.1
HM [a]	5.1	0.018	3.0
HM-80 [a]	11.2	0.04	3.8
HM-50 (fresh) [a]	24.2	0.14	10.4
HM-50 (spent)[b]	19.1	0.11	20.9
HM-20 [a]	35.6	0.17	9.9
Ni/Al_2O_3[a]	69.7	0.21	10.0

[a] unreduced & before SEGSR.
[b] after 18 adsorption-desorption cycles.

breakthrough measurements using Eq. (14). The errors in measurements were less than ± 2 %.

3. Results and discussion

3.1. Analysis of crystalline structures of hybrid materials

Fig.1 displays the XRD patterns of Ni/Al_2O_3, Ni/Li_2CuO_2, and $Ni/Al_2O_3/Li_2CuO_2$. Materials containing Ni displayed the typical NiO peaks at 43.8° and 63.6° [15,40]. The diffraction patterns for Li_2CuO_2 and fresh HM-50 (unreduced and before SEGSR) could be shown to have distinct Li_2CuO_2 peaks at 2θ of 26, 35, 39, 42, 49, 57 & 67° [37,38]. The spent HM-50 (after the 18th adsorption-desorption cycle) was found to contain Li_2CO_3 (2θ = 37, 43 & 50°) and CuO (2θ = 45, 51, 59 & 74°) phases [40,41]. Li_2O phase was also observed. The presence of Li_2CO_3 and CuO phases in the spent HM-50 endorsed Eq. (9). Table 1 lists the average crystallite sizes of various phases as determined by the Scherrer equation. After 18 sorption cycles, the NiO crystallite size increased, indicating that HM-50 had sintered during the cyclic stability test.

Table 3
Catalytic activity screening of synthesized materials by carrying out SEGSR at 700 °C, pressure = 1 bar, S/C = 6, feed flow rate = 0.5 ml/min, and GHSV = 3600 $cm^3g^{-1}h^{-1}$.

Materials	H_2 mol %
Li_2CuO_2	0
Ni/Al_2O_3	70
Ni/Li_2CuO_2 (HM)	48
$Ni/Al_2O_3/Li_2CuO_2$ (HM-80)	61
$Ni/Al_2O_3/Li_2CuO_2$ (HM-50)	94
$Ni/Al_2O_3/Li_2CuO_2$ (HM-20)	74

3.2. Analysis of textural properties of synthesized materials

Table 2 compiles the surface area and pore characteristics of all the synthesized materials. All of the materials appeared to have mesoporous structures, according to the 3.0 to 20.9 nm range in pore diameter [43]. Li_2CuO_2 had a low specific surface area (4.7 m^2/g), poor pore volume (0.017 cm^3/g), and small pore diameter (3.1 nm). This was due to its synthesis by solid-state method, which often results in dense and large particles. These findings are consistent with those of the earlier studies [40,41]. Ni/Li_2CuO_2, formed by loading 10 wt % Ni into Li_2CuO_2, had a somewhat higher surface area of 5.1 m^2/g but the same pore properties. In contrast to HM, the microstructural characteristics of HM-20, HM-50, and HM-80 greatly improved. It is evident that, as compared to HM, HM-50 has a better pore volume (0.14 cm^3/g) and an appreciable specific surface area (24.2 m^2/g). In line with expectations, the spent HM-50 had less surface area (19.9 m^2/g) and pore volume (0.11 cm^3/g) than its fresh counterpart. Moreover, after 18 cycles of adsorption and desorption, the average pore size of HM-50 rose from 10.4 nm to 20.9 nm. The increase in the average pore diameter of a material is because of the complete blockage of small pores, which reduces the number of pores available in the material.

3.3. Screening of the materials for catalytic activity

Through the steam reforming of glycerol in a fixed bed reactor, the catalytic activity of all the synthesized materials was evaluated. The reactor was loaded with 3 g of material, reduced at 515 °C for 2 h in a stream of 10 ml/min H_2 + 40 ml/min N_2 flow. Steam reforming reaction was carried out at 700 °C, S/C = 6, and a feed flow rate of 0.5 ml/min. The outcomes are shown in Table 3. All nickel-containing materials demonstrated catalytic activity. But Li_2CuO_2 by itself exhibited no catalytic activity.

Ni/Al_2O_3 has the best textural properties among the catalytically active materials, while HM has the worst (Table 2). As a result, the expected catalytic activity trend was Ni/Al_2O_3 > HM-50 > HM. However, the observed trend was HM-50 > Ni/Al_2O_3 > HM. The trend reversal between HM-50 and Ni/Al_2O_3 showed that, in addition to the textural qualities, the hybrid material's CO_2-sorption characteristics (sorption capacity and sorption kinetics) also have a significant effect on its performance.

A hybrid material's catalytic properties and adsorption characteristics are two different aspects of it. A good catalytic activity demands appreciable textural qualities. Because heterogeneous catalysis starts with the adsorption of reactants on a catalyst's surface. Thus, the low

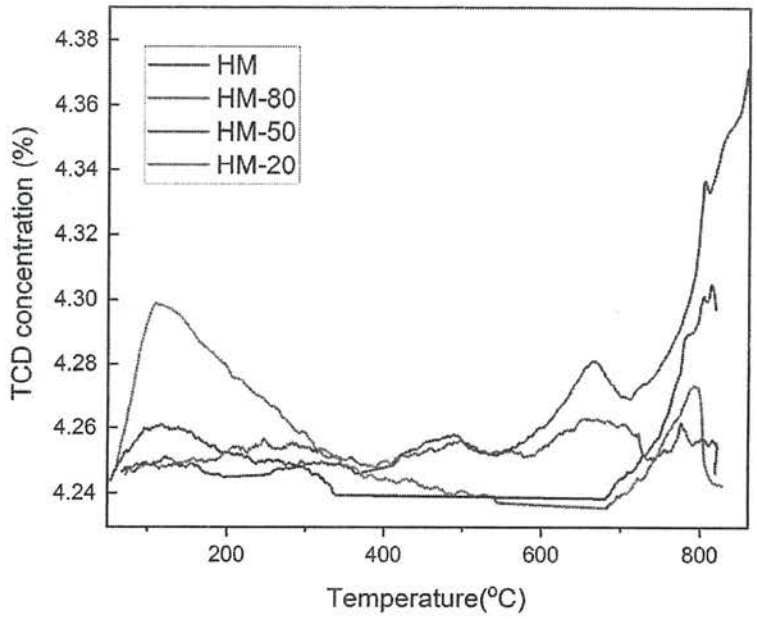

Fig. 2. CO_2-TPD profiles of the hybrid materials.

Table 4
CO_2-TPD analysis of hybrid materials.

Catalyst	Desorption temperature (°C)	Basicity of the material (mmol/g)
HM	805	0.009
HM-80	776	0.017
HM-50	813	0.212
HM-20	792	0.118

microstructural characteristics reduce the catalytic activity of a hybrid material. However, the poor microstructural characteristics do not have a significant effect on its CO_2 capture properties [40,41]. Because CO_2 is captured by a sorbent via the chemisorption mechanism, where a covalent bond is formed between CO_2 and its sorbent. In HM, HM-50, or its variants, metallic nickel is the catalytic site for SEGSR, Al_2O_3 acts as a support, and Li_2CuO_2 as support as well as CO_2 sorbent. The more the amount of Li_2CuO_2 in a hybrid material greater its adsorption capacity. Hence, greater the extent of in-situ removal of CO_2, thereby leading to the production of an enhanced purity of H_2 via SEGSR. Neither Ni nor Al_2O_3 reacts with CO_2 but their presence enhances the carbonation process [40]. On the other hand, the more the amount of Li_2CuO_2 in a hybrid material lower its microstructural characteristics. This decreases the catalytic activity of the hybrid material and decreases the glycerol conversion as well as H_2 yield. However, the more the amount of Al_2O_3 in a hybrid material greater its microstructural characteristics, thereby leading to increased catalytic activity, glycerol conversion, and H_2 yield.

While HM has low textural qualities but remarkable CO_2-sorption capabilities, Ni/Al_2O_3 has good textural qualities but no CO_2-sorption ability. By using equal weight percents of Al_2O_3 and Li_2CuO_2, it was possible to construct a trade-off between textural qualities and CO_2-sorption characteristics in HM-50. By steam reforming glycerol over Ni/Al_2O_3, about 70 mol % H_2 was produced. Such a low concentration of H_2 was due to the intrinsic equilibrium limitation of traditional steam reforming reactions as well as the high CO_2 concentration in the product gas stream. However, the in-situ adsorption of CO_2 by Li_2CuO_2 (in HM-50) was able to circumvent the restrictions of the conventional steam reforming of glycerol and produced 94 mol % H_2 under the same reaction conditions. Additionally, HM-20 and HM-80 demonstrated greater catalytic activity in comparison to HM (which contained no Al_2O_3) because the presence of Al_2O_3 enhanced their textural features. In terms of H_2 purity, HM, HM-80, and HM-20 were found to have values of 48, 61, and 74 mol %, respectively. Therefore, among all the synthesized hybrid materials, HM-50 demonstrated the best performance for H_2 generation.

The CO_2-TPD analysis results are depicted in Fig. 2. The desorption temperature and basicity of all the hybrid materials are represented in Table 4. Li_2CuO_2 undergoes decomposition at $T > 840$ °C, hence the TPD studies were followed till 830 °C. HM desorbed at 805 °C and had a basicity of 0.009 mmol/g. Al_2O_3 and Li_2CuO_2 blending increased hybrid materials' basicity as compared to that of HM, which contained no Al_2O_3. The basicity trend was found to be *HM-50 > HM-20 > HM-80 > HM*. Moreover, HM-50 exhibited a basicity of 0.212 mmol/g with a

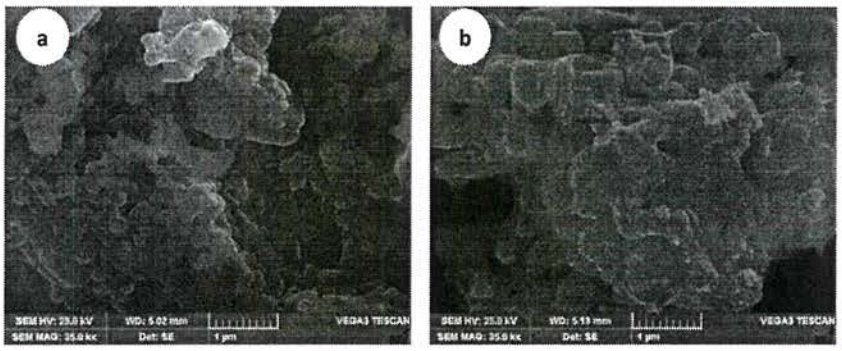

Fig. 3. SEM images of fresh HM-50 (a) and spent HM-50 (b).

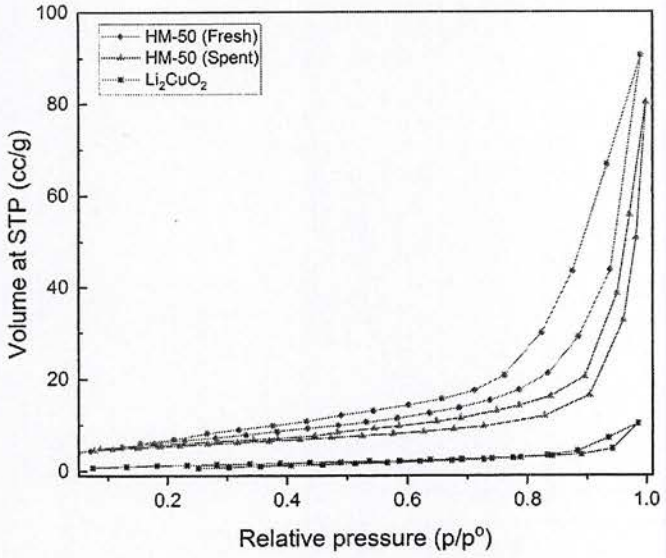

Fig. 4. N_2 adsorption-desorption isotherms.

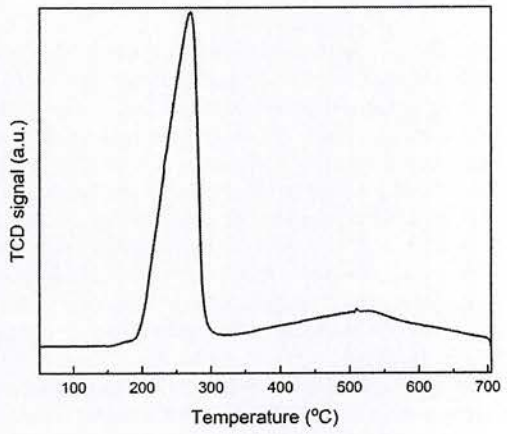

Fig. 5. H_2-TPR profile of HM-50.

Table 5
Binding energies (in eV) associated with lines obtained from XPS spectra.

Sample	Lithium	Aluminium		Oxygen	Nickel		Copper	
	1s	2s	2p	1s	$2p_{3/2}$	$2p_{1/2}$	$2p_{3/2}$	$2p_{1/2}$
HM-50 (fresh)	55	119	74	531	856	872	934	953
HM-50 (spent)	56	119	75	532	855	875	934	953

desorption temperature of 813 °C. The adsorption of CO_2, an acidic gas, is facilitated by a more basic substance. In order to effectively collect CO_2, a bifunctional material utilized to produce high-purity H_2 through sorption-enhanced reforming processes must have a sizable basicity. Because of HM-50's greater basicity, it was possible to generate high purity (94 mol %) H_2 at 700 °C via SEGSR.

The SEM images of the fresh and spent HM-50 are shown in Fig. 3. Pore properties (Table 2) and the isothermal N_2 adsorption-desorption curves (Fig. 4) indicated that the materials were not non-porous but rather had a low degree of porosity.

The N_2 adsorption-desorption isotherms for Li_2CuO_2, fresh HM-50, and spent HM-50 are shown in Fig. 4. They were all type III isotherms, but each had a different hysteresis loop [45]. Li_2CuO_2 particles were dense, big, and nonporous, as shown by a very narrow H3-type hysteresis loop. Solid-state processes frequently result in the production of these kinds of particles. A higher hysteresis loop of type H3 suggested that both the fresh and spent HM-50 had some kind of porosity. After 18 adsorption-desorption cycles, the spent HM-50 isotherm showed a shrinking of the hysteresis loop, which indicated that the HM-50's porosity had decreased.

In Fig. 5, an H_2-TPR profile of the HM-50, which was calcined at 700 °C, is shown. In the TPR profile, two peaks can be seen. 270 °C marked the first peak, and 515 °C the second. Lower temperatures led to the reduction of the bulk NiO, which had little interaction with the support, but higher temperatures led to the reduction of the surface NiO, which had a strong interaction with the support [45,46]. In order to prepare HM-50 for the SEGSR reactions, it was reduced at 515 °C.

The H_2-pulse chemisorption analysis of HM-50 indicated the 5.3 % dispersion of Ni with 18.2 μg/mol of H_2 uptake. A good dispersion of active metal on the support enhances the catalytic activity of the material. By using EDX analysis, it was discovered that fresh HM-50's consisted of 13.8 wt % Ni, 25.6 wt %Cu, 27.3 wt % Al, and 33.3 wt % O.

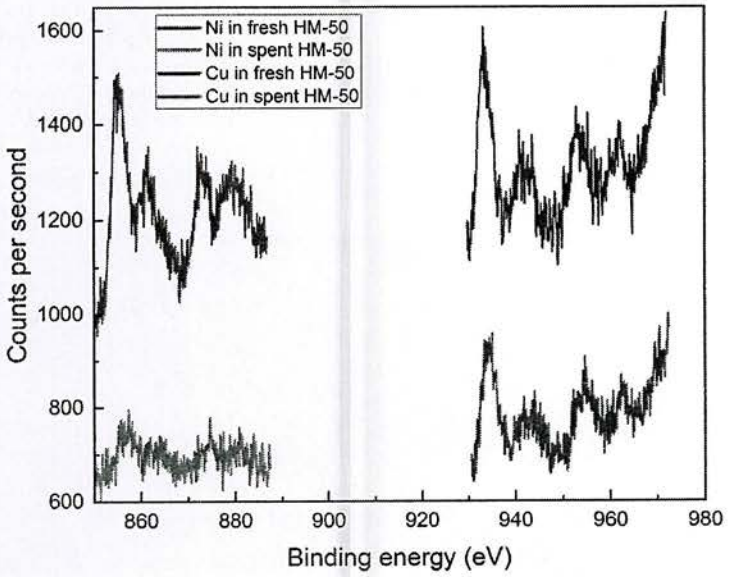

Fig. 6. XPS spectra showing Ni and Cu peaks.

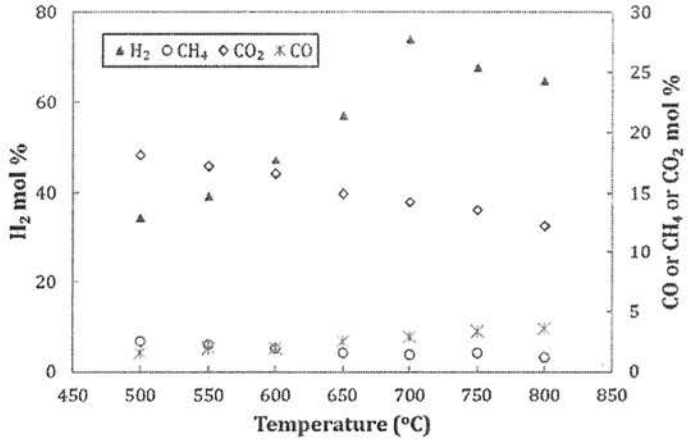

Fig. 7. Product gas composition (mol %), on a dry basis under the steady state conditions, as a function of reaction temperature for steam reforming of glycerol over HM-50 at S/C = 6 and feed flow rate = 0.5 ml/min.

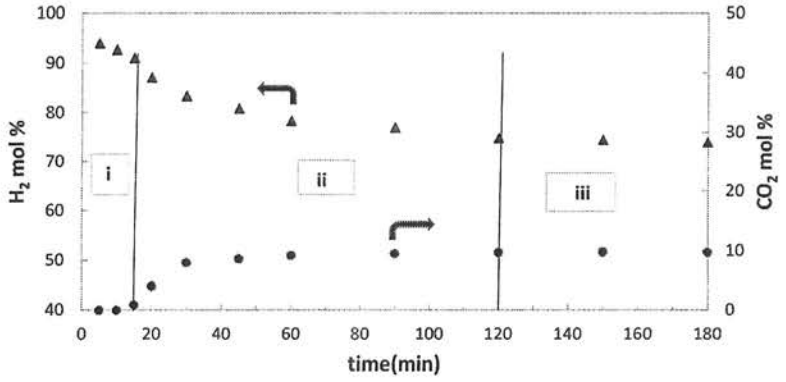

Fig. 8. Breakthrough curve for the SEGSR over HM-50 (reaction conditions: Temperature = 700 °C, pressure = 1 bar, feed flow = 0.5 ml/min, S/C = 6 mol/mol, and time on stream = 3 h). *i – pre-breakthrough stage; ii – breakthrough stage; iii – post-breakthrough stage.*

Li cannot be detected by EDX, hence its wt % is missing.

The results of the XPS analysis of the fresh and spent HM-50 are summarized in Fig.6 and Table 5. The binding energy values for 2p electrons of Ni in fresh HM-50 were found to be 856 and 872 eV respectively for triplet ($2p_{3/2}$) and singlet states ($2p_{1/2}$). Cu also exhibited similar behaviour but with higher binding energy values 934 for $2p_{3/2}$ and 953 for $2p_{1/2}$ states. Similar trend was also observed in the spent HM-50. Thus, indicating that Ni and Cu ions experienced two different chemical environments in fresh as well as spent hybrid materials. These results are in line with the reported values [41]. XPS studies also quantified 10.3 and 8.6 mass percent of Ni in the fresh and spent HM-50, respectively.

3.4. Product gas compositions at steady state

Glycerol was steam-reformed over HM-50 in the temperature range of 500 °C to 800 °C. The outcomes under steady-state conditions are shown in Fig. 7.

It was observed that the reaction produced four products (H_2, CO, CH_4 & CO_2) in the gas phase and one product, acetaldehyde (CH_3CHO), in the liquid phase. The concentration of H_2 increases as the reaction temperature rises from 500 to 700 °C, but when the temperature rises further, the concentration of H_2 declines. On the other hand, as the temperature rises, the concentration of CH_4 and CO_2 falls. In contrast, when the temperature of reforming rises, the concentration of CO continues to rise. This may be caused by the ascendency of the RWGS reaction, Eq. (8), and the methane reforming, Eqs. (6) & (7), at higher temperatures.

3.5. SEGSR over HM-50

Fig. 8, depicts a typical concentration versus time graph at a specific temperature (700 °C). It illustrates how the concentration of H_2 decreases as the reaction advances and the concentration of CO_2 increases until an equilibrium (a steady state) is attained. The concentrations of CO and CH_4 (not shown) likewise exhibit a tendency similar to that of CO_2.

Like any SERP, the SEGSR reaction went through three distinct phases, which are shown in Fig. 8. *Pre-breakthrough stage* and sorption-enhanced steam reforming (SESR) stage are two names for the initial reaction stage [15,19]. It is a CO_2-free stage because HM-50 completely removes all CO_2 produced during this stage of the reaction. Furthermore, the concentration of H_2 is maximized when CO_2 is not present in the exit gas stream. This phase lasts until the breakthrough time (t_b), which occurs when CO_2 starts to appear in the outflow stream for the first time after the reaction starts. The proportion of H_2 in the outflow stream gradually drops as the reaction progresses, while that of other products gradually rises. The second phase is referred to as the *breakthrough phase*. It begins at the breakthrough time and lasts until the reaction reaches equilibrium. This stage is characterized by a rise in the CO_2 concentration and a fall in the H_2 concentration in the output stream. At this point, the CO_2 sorbent is almost saturated. This phase sees the change from SESR to steam reforming (SR). The *post-breakthrough stage*, often referred to as the SR stage, is the third stage. The sorbent becomes entirely saturated during the equilibrium stage, at which point the concentration of each species is constant. The hybrid material's sorption characteristics alter over the stages, but its reforming

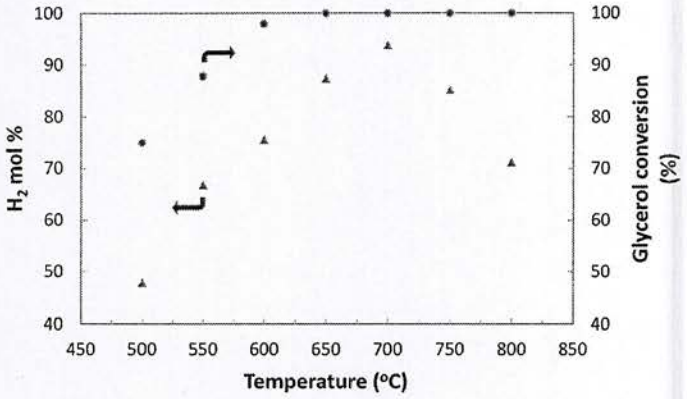

Fig. 9. Effect of temperature on SEGSR over HM-50 (reaction conditions: temperature = 500–800 °C, pressure = 1 bar, S/C = 6 mol/mol, feed flow = 0.5 ml/min).

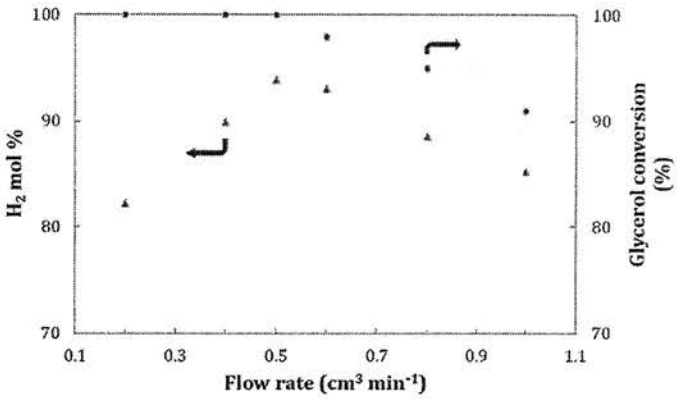

Fig. 10. Effect of feed flow rate on SEGSR over HM-50 (reaction conditions: temperature = 700 °C, pressure = 1 bar, S/C = 6, GHSV = 3600 cm^3 g^{-1} h^{-1}, time on stream = 3 h).

Table 6
The effect of temperature on the breakthrough time and adsorption capacity of HM-50. (Reaction conditions: T = 500–800 °C, p = 1 bar, S/C = 6 mol/mol, feed flow = 0.5 ml/min, GHSV = 3600 $cm^3 g^{-1} h^{-1}$, time on stream =3 h).

Temperature (°C)	t_b @ (min)	Q_{ads} # (mmol CO_2 / g HM-50)
500	25	1.9 (8.2)$
550	20	2.3 (10.2)
600	15	3.0 (13.2)
650	15	3.5 (15.3)
700	15	3.9 (16.9)
750	10	2.9 (12.8)
800	05	1.7 (7.6)

@ Determined from gas chromatograms.
# Calculated by Eq. (14).
$ wt % values are given in parentheses.

activity stays the same [19]. According to Fig. 8, the reaction, which had a 15-minute breakthrough time, reached equilibrium within 3 h of being in operation. Consequently, each reforming reaction was run for three hours only.

3.6. Effect of temperature on SEGSR

The impact of temperature change between 500 and 800 °C on SEGSR over HM-50 is summarized in Fig. 9. Glycerol conversion was seen to increase from 75 % at 500 °C to 100 % at temperatures > 600 °C. It was due to the endothermic nature of all reforming reactions, Eq. (1). The increased glycerol conversion resulted in the production of more H_2 and CO_2. Raising the reaction temperature from 500 °C to 700 °C resulted in an increase in the concentration of H_2 from 48 mol % to 94 mol %. Further increase in the reaction temperature decreased the concentration of H_2 to 85 mol % and 71 mol % at 750 °C and 800 °C, respectively. These findings are attributable to the fact that Li_2CuO_2's ability for CO_2 adsorption rises with temperature up to 700 °C but at T > 700 °C, nevertheless, it shows desorption. Therefore, 700 °C was considered the optimal temperature for SEGSR over HM-50.

3.7. Determination of CO_2 adsorption capacity of HM-50

In Table 6, the breakthrough time (t_b) and adsorption capacity (Q_{ads}) of HM-50 at various temperatures are given. As anticipated, t_b dropped as the reaction temperature rose. Higher reaction temperatures caused the enhanced glycerol conversion to produce more and more CO_2, which accelerated the saturation of the available adsorbing sites on HM-50. The maximum breakthrough time of 25 min was recorded at 500 °C having an H_2 concentration of roughly 48 mol %. However, the catalyst

stream contained 94 mol % H_2 at the optimal reaction temperature (700 °C), with a t_b of 15 min.

Being a high-temperature (> 400 °C) CO_2-sorbent, Li_2CuO_2 exhibits a maximum adsorption capacity of 9.1 mmol CO_2/g (or 40.21 wt. %) [40,41]. Therefore, HM-50, which contains 45 wt % Li_2CuO_2 has a theoretical adsorption capacity of about 4.1 mmol CO_2/g. In this investigation, HM-50 demonstrated its exceptional sorption characteristics with an adsorption capacity of 3.9 mmol CO_2/g (around 95 % of its theoretical adsorption capacity) at the optimum reaction temperature of 700 °C.

When the reaction temperature was increased from 500 to 700 °C, the HM-50's CO_2-adsorption capacity increased from 1.9 to 3.9 mmol CO_2/g (Table 6). In other words, when the temperature rose, so did the material's adsorption capacity. Similar patterns were seen in earlier works too [15,21,39–41]. The two-step mechanism of CO_2 chemisorption on alkali metal ceramics [24,34] provides an explanation for the behavior of HM-50 in question. The first phase is the superficial reaction phase, while the second is the bulk diffusion phase. Alkali metal carbonate, Li_2CO_3 in this case, Eq. (9), which forms an outer shell around the material, is formed in the first stage when CO_2 combines with the alkali metals that are already present on the substance's surface. This process happens at a lower temperature (till 400 °C). In the bulk diffusion phase (T > 400 °C), the chemisorption is continued by the diffusion of CO_2 molecules through the alkali carbonate shell to the core or the diffusion of alkali metal ions and oxide ions from the unreacted core to the surface (via the alkali carbonate shell). Ions/CO_2 diffusion is the step that determines the rate of the sorption process, and it plays a significant role in chemisorption [29,30,34]. A rise in temperature speeds up the diffusion process by creating the molten liquid phase of alkali metal carbonate. As a result, an increase in temperature increases the HM-50's CO_2 chemisorption properties, which seem to have stopped at lower temperatures. Hence, with a rise in temperature, the adsorption capacity of HM-50 increases till desorption becomes prominent at T > 700 °C. Therefore, the adsorption capacity of HM-50 decreased to 2.9 and 1.7 mmol/g at 750 and 800 °C, respectively. Hence the optimum sorption temperature of HM-50 was found to be 700 °C, the same as the optimal reaction temperature for SEGSR.

3.8. Effect of the feed flow rate on SEGSR

The performance of the HM-50 is also impacted by the feed flow rate. A number of reactions were conducted to better understand the same by changing the flow rate of glycerol solution from 0.2 to 1.0 cm^3 min^{-1}. Fig. 10 presents the findings. More glycerol molecules enter the reactor in a given amount of time the higher the feed flow rate. Up to a feed flow rate of 0.5 cm^3 min^{-1}, 100 % glycerol conversion was seen. To put it another way, the loaded amount (3 g) of HM-50 was able to interact with

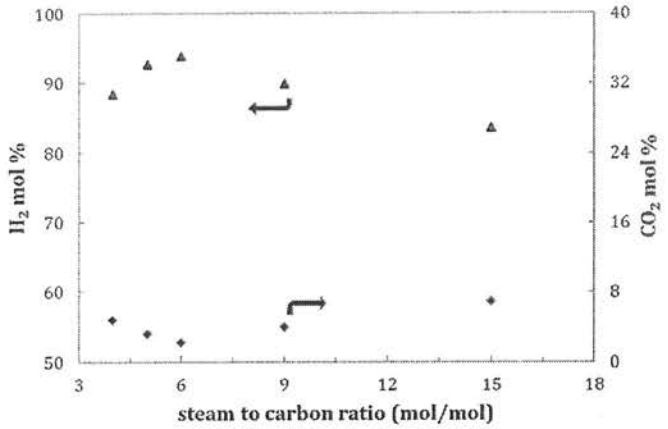

Fig. 11. Effect of S/C on SEGSR over HM-50 (reaction conditions: temperature =700 °C, pressure = 1 bar, feed flow = 0.5 cm^3 min^{-1}, GHSV = 3600 cm^3 g^{-1} h^{-1}, time on stream = 3 h).

every molecule of glycerol that passed over it every time and turn them into products. The glycerol conversion reduced as the flow rate increased, going from 98 % at 0.6 cm^3 min^{-1} to 91 % at 1.0 cm^3 min^{-1}, showing that not all of the glycerol molecules traveling over HM-50 could be converted to product. When the feed flow was greater than 0.5 cm^3 min^{-1}, the amount of HM-50 loaded was not sufficient to interact with all of the glycerol molecules entering the reactor per unit time, causing a small number of glycerol molecules to escape the catalytic bed unreacted. Similar to this, the increased feed flow rate from 0.2 to 0.5 cm^3 min^{-1}, resulted in an increase in the H_2 concentration from 82 to 94 mol %. A feed flow rate greater than 0.5 cm^3 min^{-1}, however, caused it to decline. Since the concentration of CO_2 became noticeably diluted at a high feed flow rate, its in-situ adsorption was reduced. Additionally, the glycerol conversion was reduced at a higher flow rate, thereby decreasing the H_2 mol %. Therefore, the optimal feed flow rate for SEGSR over 3 g of HM at 700 °C was determined to be 0.5 cm^3 min^{-1}.

3.9. Effect of S/C on SEGSR

A catalyst typically becomes inactive during reforming processes as a result of carbon buildup on its surface. Carbon is created either through CO disproportionation ($2CO \rightleftharpoons C(s) + CO_2$) or CH_4 breakdown ($CH_4 \rightleftharpoons C(s) + 2H_2$), or both [14,18,43]. Coke formation is slowed by a high S/C [9]. Additionally, it was discovered that the CO_2-sorption process was facilitated by the presence of water vapor [41]. At 700 °C, p = bar, and feed flow = 0.5 cm^3 min^{-1}, S/C was altered from 4 to 15 to evaluate its impact on the performance of HM-50. Fig. 11 presents the findings. The concentration of CO_2 was reduced from 4.8 to 2.2 mol % due to the rise in S/C from 4 to 6. As a result, the concentration of H_2 has increased from 88 mol % at S/C = 4 to 94 mol % at S/C = 6. Additionally, as S/C rose further, the concentration of H_2 dropped to 89 mol % at S/C = 9 and 84 mol % at SC=15. Because the partial pressure of CO_2 becomes remarkably low at notably high S/C, its adsorption is reduced. As a result, at greater S/C, the outlet gas stream's CO_2 concentration increases and its H_2 concentration decreases. S/C = 6 was therefore thought to be the best value for the current work.

3.10. Effect of gas hourly space velocity (GHSV) on SEGSR

The adsorption capacity and catalytic activity of a hybrid material also depend on the amount of it is placed in a reactor. The capacity to adsorb CO_2 increases with increasing loading amounts, which results in a higher concentration of H_2 being generated [15]. Our reactor has a material holding capacity of 3 g. Therefore, the ideal quantity of HM-50 employed for this study was 3 g, which corresponded to the GHSV of 3600 $cm^3g^{-1}h^{-1}$.

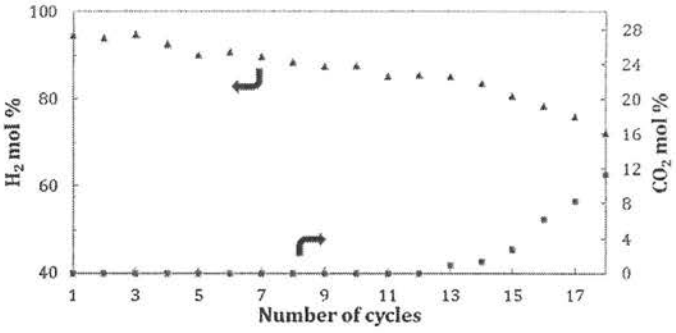

Fig. 12. Cyclic stability study of HM-50 on SEGSR (reaction conditions: temperature = 700 °C, pressure = 1 bar, S/C = 6 mol/mol, feed flow = 0.5 m//min, GHSV = 3600 $cm^3g^{-1}h^{-1}$; regeneration conditions: (N_2 + steam) flow at (80+02) ml/min, temperature = 700 °C).

3.11. Regeneration and cyclic stability of HM-50

The multi-cycle stability of a catalyst is one of the key parameters required for its industrial applications. It can be assessed by monitoring the concentration of H_2 produced over a number of cycles. Each cycle for this study lasted 60 min and included 30 min for high-purity H_2 production (CO_2 adsorption), followed by 30 min for regeneration (CO_2 desorption). Adsorption processes were conducted at T = 700 °C, p = 1 bar, S/C = 6, feed flow = 0.5 ml/min, GHSV = 3600 cm^3 g^{-1} h^{-1}, and N_2 flow = 40 ml/min. A mixture of N_2 (80 ml/min) and steam (2 ml/min) was passed at 700 °C to carry out the desorption process. The appearance and disappearance of CO_2 in the TCD signals served as indicators of the carbonation and regeneration responses, respectively. Fig. 12 shows the outcomes of the same.

The highest H_2 concentration during the pre-breakthrough stage and the CO_2 concentration at breakthrough time (t_b = 15 min, Fig. 8) for each cycle are plotted in Fig.12. It is clear that up to the 13th cycle, the H_2 concentration was more than 85 mol %. But, in the 16th cycle, it decreased below 80 mol %. Nevertheless, after the 18th cycle it reached around 73 mol %, the same as that at the steady-state condition at 700 °C (Fig. 7). Similarly, till the 12th cycle, CO_2 started appearing in the outlet stream after 15 min. However, from the 13th cycle onwards it started appearing even before 15 min. Moreover, it appeared in the outlet stream within no time during the 18th cycle. This was due to the sintering of HM-50 causing a gradual loss of its sorption properties and irreversible structural changes.

3.12. Structural changes in HM-50

The performance of HM-50 decreased appreciably after 18 cycles of carbonation-regeneration. The leading cause was due to the change in the textural properties as well as the loss of sorption characteristics of HM-50. The surface area as well as the total pore volume decreased by 21 % each (Table 2). This led to a decrease in the catalytic activity of HM-50. Thus, decreasing the glycerol conversion and H_2 production. As discussed earlier, the decrease in the textural characteristics of HM-50 did not have a significant effect on its CO_2 sorption characteristics [40]. However, it was observed in Fig. 12 that during the 18th cycle, CO_2 started appearing in the outlet stream within no time. In other words, after the 17th carbonation-calcination cycle, HM-50 entirely lost its sorption characteristics. XRD pattern of spent HM-50 (Fig. 1) confirmed the presence of Li_2CO_3 and CuO crystallite phases but the absence of the Li_2CuO_2 phase in it. It means from the 13th cycle (Fig. 12), Li_2CuO_2 gradually lost its reversibility, Eq. (9), and became completely irreversible after the 17th cycle. This irreversible structural change transitioned the reaction from SESR to SR. Hence, the performance of the hybrid material decreased significantly after the 17th cycle. The SEM images of HM-50 (Fig. 3) clearly indicate the aggregation of particles

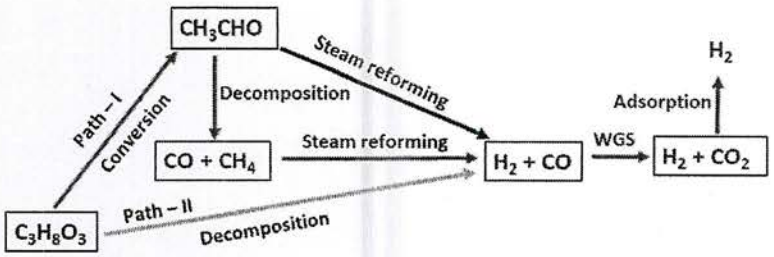

Fig. 13. Plausible reaction pathways (green arrows) for SEGSR over HM-50.

due to sintering during the cyclic stability test. The narrowing of the hysteresis loop in Fig. 4 supplements the same.

3.13. Probable reaction mechanism

Glycerol steam reforming often proceeds along one of the two paths [12,14,15,21,29], as depicted in Fig. 13. Glycerol ($C_3H_8O_3$) is catalytically transformed to acetaldehyde (CH_3CHO), Eq. (15), in the first pathway (Path - I), from which it either form H_2 & CO, via steam reforming, Eq. (16) or decomposes to CH_4 & CO, Eq (17). The second pathway (Path - II) involves the direct breakdown of glycerol into syngas ($H_2 + CO$), Eq (2). Further, CH_4 goes through steam reforming to generate extra H_2 and CO, Eq (6). All the stages' CO output results in the WGS reaction, which produces H_2 and CO_2, Eq (3). Subsequently, high-purity H_2 is produced as a result of the in-situ adsorption of CO_2.

Formation of acetaldehyde: $C_3H_8O_3 \rightleftharpoons CH_3CHO + H_2 + CO + H_2O$ (15)

Steam reforming of acetaldehyde: $CH_3CHO + H_2O \rightleftharpoons 3H_2 + 2CO$ (16)

Decomposition of acetaldehyde: $CH_3CHO \rightleftharpoons CH_4 + CO$ (17)

Four gas phase products (H_2, CO, CH_4 & CO_2) were detected by TCD-GC during the SEGSR over HM-50. Acetaldehyde was the sole liquid product found in this investigation using FID-GC, and it was only found at low reaction temperatures ($T \leq 600$ °C). Its detection revealed that the reactions followed the path – I. The liquid fractions did not contain any acetaldehyde, nevertheless, when the reactions were conducted at $T > 600$ °C. It might be caused by the quick steam reformation or decomposition of CH_3CHO that occurs at higher temperatures. Moreover, as shown in Fig. 7, when the temperature was elevated from 500 °C to 800 °C, the concentration of CO increased from 1.5 to 3.6 mol % and that of CH_4 fell from 2.5 to 1.2 mol %. The direct breakdown of glycerol (i.e. path-II) to H_2 and CO does not appear to be supported by the low concentration of CO in the exit gas stream. Because it would have produced more amount of CO and no CH_4 according to Eq. (2), which suggested the production of 3 mol of CO by the decomposition of 1 mol of glycerol. Again, the discouragement of WGS reaction, Eq. (3), with a rise in temperature would have led to a significant increase in CO concentration had there been direct decomposition of glycerol. Additionally, since both the methanation reactions, Eqs. (4) and (5) are highly exothermic and less favorable at higher temperatures, these reactions cannot produce CH_4 at T > 500 °C [14,42,47]. Furthermore, the presence of CH_4 in the outlet gas stream sounds to support the rapid decomposition of CH_3CHO to CH_4 and CO, Eq. (17) rather than steam reforming of CH_3CHO to produce 2 mol of CO (and no CH_4) per mol of it reacted, Eq. (16). Higher temperature promoted the SMR, thereby decreasing the concentration of CH_4 with an increase in reaction temperature. Thus, the plausible mechanism of the SEGSR over HM-50 was the catalytic conversion of glycerol to acetaldehyde followed by the rapid decomposition of the latter to CO and CH_4. Thereafter, subsequent SMR, WGS, and CO_2 adsorption led to the production of high-purity H_2. The presence of Ni and Cu in HM-50 facilitated dehydrogenation and C—C bond cleavage [15]. Cu also promoted WGS reaction [15,29].

4. Conclusion

In a continuous fixed-bed down-flow reactor, glycerol was catalytically converted to H_2 via a sorption-enhanced steam reforming process. Among all the synthesized catalytic materials, the hybrid material HM-50, which contained 10 wt % Ni and equal wt % of Al_2O_3 and Li_2CuO_2 performed the best. Investigations were carried out, at atmospheric pressure, in the temperature range of 500 to 800 °C, feed flow rate of 0.2 to 1.0 ml/min, and S/C of 4 to 15 mol/mol. 100 % glycerol conversion, 90 % H_2 yield, 94 mol % H_2 purity, and adsorption capacity of 3.9 mmol CO_2 per gram of material were observed at the optimum reaction conditions: $T = 700$ °C, feed flow rate = 0.5 ml/min, and S/C = 6. With a breakthrough time of 15 min, HM-50 produced > 85 mol % pure H_2 till the 13th sorption cycle. Each sorption cycle consisted of 30 min of reforming reaction followed by 30 min for regeneration. The regeneration of the material by was carried out by passing a mixture of 80 ml/min N_2 gas and 2 ml/min steam at 700 °C. A most plausible reaction mechanism indicated the conversion of glycerol to acetaldehyde followed by the decomposition of the latter to CO and CH_4. Subsequently, SMR, WGS, and CO_2 adsorption by HM-50 produced high-purity H_2. The performance of HM-50 for SEGSR was comparable to the works published by other researchers, as can be seen in Table S1 (supplementary material). The impressive performance of HM-50 makes it a potential bifunctional material for the production of fuel cell grade H_2 by sorption-enhanced steam reforming processes.

CRediT authorship contribution statement

Prabijna S.S. Babu: Conceptualization, Methodology, Investigation, Writing – original draft. **Prakash D. Vaidya:** Supervision, Resources, Writing – review & editing.

Declaration of Competing Interest

The authors declare that they have no known competing financial interests or personal relationships that could have appeared to influence the work reported in this paper.

Data availability

Data will be made available on request.

Acknowledgments

We appreciate the work done in characterizing our materials by the staff at the Material Analysis and Research Center, BIT Bengaluru (India), the Department of Physics, ICT Mumbai and CE XPS Facility of ICT Mumbai.

Supplementary materials

Supplementary material associated with this article can be found, in the online version, at doi:10.1016/j.mcat.2023.113718.

References

[1] National Portal of India. https://www.india.gov.in/spotlight/national-green-hydrogen-mission, 2023 (Accessed 30 May 2023).

[2] T. Capurso, M. Stefanizzi, M. Torresi, S.M. Camporeale, Perspective of the role of hydrogen in the 21st century energy transition,, Energy Convers. Manag. (2022) 251, https://doi.org/10.1016/j.enconman.2021.114898.

[3] S.E. Hosseini, M.A. Wahid, Hydrogen production from renewable and sustainable energy resources: promising green energy carrier for clean development, Renew. Sustain. Energy Rev. 57 (2016) 850–866, https://doi.org/10.1016/j.rser.2015.12.112.

[4] N. de Miguel, J. Manzanedo, P.L. Arias, Testing of a Ni-Al_2O_3 catalyst for methane steam reforming using different reaction systems, Chem. Eng. Technol. 35 (2012) 720–728, https://doi.org/10.1002/ceat.201100348.

[5] I. Dincer, C. Acar, Review and evaluation of hydrogen production methods for better sustainability, Int. J. Hydrogen Energy 40 (2014) 11094–11111, https://doi.org/10.1016/j.ijhydene.2014.12.035.

[6] E.L.G. Oliveira, C.A. Grande, A.E. Rodrigues, Effect of catalyst activity in SMR-SERP for hydrogen production: commercial vs. large-pore catalyst, Chem. Eng. Sci. 66 (2011) 342–354, https://doi.org/10.1016/j.ces.2010.10.030.

[7] D. Chen, L. He, Towards an efficient hydrogen production from biomass: a review of processes and materials, ChemCatChem 3 (2011) 490–511, https://doi.org/10.1002/cctc.201000345.

[8] D. Li, X. Li, J. Gong, Catalytic Reforming of oxygenates: state of the art and future prospects, Chem. Rev. 116 (2016) 11529–11653, https://doi.org/10.1021/acs.chemrev.6b00099.

[9] P.D. Vaidya, A.E. Rodrigues, Glycerol reforming for hydrogen production: a review, Chem. Eng. Technol. 32 (2009) 1463–1469, https://doi.org/10.1002/ceat.200900120.

[10] M.S. Macedo, M.A. Soria, L.M. Madeira, Process intensification for hydrogen production through glycerol steam reforming, Renew. Sustain. Energy Rev. 146 (2021), https://doi.org/10.1016/j.rser.2021.111151.

[11] N.A. Roslan, S.Z. Abidin, A. Ideris, D.V.N. Vo, A review on glycerol reforming processes over Ni-based catalyst for hydrogen and syngas productions, Int. J. Hydrogen Energy 45 (2020) 18466–18489, https://doi.org/10.1016/j.ijhydene.2019.08.211.

[12] S. Adhikari, S.D. Fernando, A. Haryanto, Hydrogen production from glycerol: an update, Energy Convers. Manag. 50 (2009) 2600–2604, https://doi.org/10.1016/j.enconman.2009.06.011.

[13] H. Chen, Y. Ding, N.T. Cong, B. Dou, V. Dupont, M. Ghadiri, P.T. Williams, A comparative study on hydrogen production from steam-glycerol reforming: thermodynamics and experimental, Renew. Energy 36 (2011) 779–788, https://doi.org/10.1016/j.renene.2010.07.026.

[14] B. Dou, C. Wang, Y. Song, H. Chen, Y. Xu, Activity of Ni-Cu-Al based catalyst for renewable hydrogen production from steam reforming of glycerol, Energy Convers. Manag. 78 (2014) 253–259, https://doi.org/10.1016/j.enconman.2013.10.067.

[15] K.D. Dewoolkar, P.D. Vaidya, Sorption-Enhanced steam reforming of glycerol over Ni–hydrotalcite: effect of promotion with Pt, ChemCatChem 8 (2016) 3499–3509, https://doi.org/10.1002/cctc.201600793.

[16] B. Jiang, L. Li, Z. Bian, Z. Li, Y. Sun, Z. Sun, D. Tang, S. Kawi, B. Dou, M.A. Goula, Chemical looping glycerol reforming for hydrogen production by Ni@ZrO_2 nanocomposite oxygen carriers, Int. J. Hydrogen Energy 43 (2018) 13200–13211, https://doi.org/10.1016/j.ijhydene.2018.05.065.

[17] F. Qureshi, M. Yusuf, A.A. Pasha, H.W. Khan, B. Imteyaz, K. Irshad, Sustainable and energy efficient hydrogen production via glycerol reforming techniques: a review, Int. J. Hydrogen Energy 47 (2022) 41397–41420, https://doi.org/10.1016/j.ijhydene.2022.04.010.

[18] M.S. Macedo, M.A. Soria, L.M. Madeira, Glycerol steam reforming for hydrogen production: traditional versus membrane reactor, Int. J. Hydrogen Energy 44 (2019) 24719–24732, https://doi.org/10.1016/j.ijhydene.2019.07.046.

[19] C. Wang, B. Dou, H. Chen, Y. Song, Y. Xu, X. Du, L. Zhang, T. Luo, C. Tan, Renewable hydrogen production from steam reforming of glycerol by Ni-Cu-Al, Ni-Cu-Mg, Ni-Mg catalysts, Int. J. Hydrogen Energy 38 (2013) 3562–3571, https://doi.org/10.1016/j.ijhydene.2013.01.042.

[20] A.Z. Senseni, F. Meshkani, M. Rezaei, Steam reforming of glycerol on mesoporous nanocrystalline Ni/Al_2O_3 catalysts for H_2 production, Int. J. Hydrogen Energy 41 (2016) 20137–20146, https://doi.org/10.1016/j.ijhydene.2016.08.046.

[21] C. Wang, Y. Chen, Z. Cheng, X. Luo, L. Jia, M. Song, B. Jiang, B. Dou, Sorption-enhanced steam reforming of glycerol for hydrogen production over a NiO/$NiAl_2O_4$ catalyst and Li_2ZrO_3-based sorbent, Energy Fuels 29 (2015) 7408–7418, https://doi.org/10.1021/acs.energyfuels.5b01941.

[22] Y. Wang, M.Z. Memon, M.A. Seelro, W. Fu, Y. Gao, Y. Dong, G. Ji, A review of CO_2 sorbents for promoting hydrogen production in the sorption-enhanced steam reforming process, Int. J. Hydrogen Energy 46 (2021) 23358–23379, https://doi.org/10.1016/j.ijhydene.2021.01.206.

[23] M.Z. Memon, X. Zhao, V.S. Sikarwar, A.K. Vuppaladadiyam, S.J. Milne, A. P. Brown, J. Li, M. Zhao, Alkali metal CO_2 sorbents and the resulting metal carbonates: potential for process intensification of sorption-enhanced steam reforming, Environ. Sci. Technol. 51 (2017) 12–27, https://doi.org/10.1021/acs.est.6b04992.

[24] M. Shokrollahi Yancheshmeh, H.R. Radfarnia, M.C. Iliuta, High temperature CO_2 sorbents and their application for hydrogen production by sorption enhanced steam reforming process, Chem. Eng. J. 283 (2016) 420–444, https://doi.org/10.1016/j.cej.2015.06.060.

[25] G. Ji, H. Yang, M.Z. Memon, Y. Gao, B. Qu, W. Fu, G. Olguin, M. Zhao, A. Li, Recent advances on kinetics of carbon dioxide capture using solid sorbents at elevated temperatures, Appl. Energy 267 (2020), 114874, https://doi.org/10.1016/j.apenergy.2020.114874.

[26] M.J. Hsu, K.H. Lee, Y.P. Chyou, CO_2 capture at high temperature using calcium-based sorbents, J. Chin. Inst. Eng., Trans. Chin. Inst. Eng., Series A 37 (2014) 152–164, https://doi.org/10.1080/02533839.2012.757045.

[27] Y. Ding, E. Alpay, Equilibria and kinetics of CO_2 adsorption on hydrotalcite adsorbent, Chem. Eng. Sci. 55 (2000) 3461–3474, https://doi.org/10.1016/S0009-2509(99)00596-5.

[28] S. Sang, Z.J. Zhao, H. Tian, Z. Sun, H. Li, S. Assabumrungrat, T. Muhammad, L. Zeng, J. Gong, Promotional role of MgO on sorption-enhanced steam reforming of ethanol over Ni/CaO catalysts, AIChE J. 66 (2020), https://doi.org/10.1002/aic.16877.

[29] S.A. Ghungrud, P.D. Vaidya, Sorption-enhanced reaction process for glycerol-to-hydrogen conversion over cobalt catalyst supported on promoted hydrotalcites, Int. J. Hydrogen Energy 45 (2020) 9440–9450, https://doi.org/10.1016/j.ijhydene.2020.01.206.

[30] A.F. Cunha, Y.J. Wu, F.A. Díaz Alvarado, J.C. Santos, P.D. Vaidya, A.E. Rodrigues, Steam reforming of ethanol on a Ni/Al_2O_3 catalyst coupled with a hydrotalcite-like sorbent in a multilayer pattern for CO_2 uptake, Can. J. Chem. Eng. 90 (2012) 1514–1526, https://doi.org/10.1002/cjce.20662.

[31] K. Essaki, T. Muramatsu, M. Kato, Effect of equilibrium shift by using lithium silicate pellets in methane steam reforming, Int. J. Hydrogen Energy 33 (2008) 4555–4559, https://doi.org/10.1016/j.ijhydene.2008.05.063.

[32] N. Wang, Y. Feng, Y. Chen, X. Guo, Lithium-based sorbent from rice husk materials for hydrogen production via sorption-enhanced steam reforming of ethanol, Fuel 245 (2019) 263–273, https://doi.org/10.1016/j.fuel.2019.02.048.

[33] E. Ochoa-Fernández, H.K. Rusten, H.A. Jakobsen, M. Rønning, A. Holmen, D. Chen, Sorption enhanced hydrogen production by steam methane reforming using Li_2ZrO_3 as sorbent: sorption kinetics and reactor simulation, Catal. Today 106 (2005) 41–46, https://doi.org/10.1016/j.cattod.2005.07.146.

[34] C. Wang, B. Dou, Y. Song, H. Chen, Y. Xu, B. Xie, High temperature CO_2 sorption on Li_2ZrO_3 based sorbents, Ind. Eng. Chem. Res. 53 (2014) 12744–12752, https://doi.org/10.1021/ie502042p.

[35] J.A. Mendoza-Nieto, Y. Duan, H. Pfeiffer, Alkaline zirconates as effective materials for hydrogen production through consecutive carbon dioxide capture and conversion in methane dry reforming, Appl. Catal. B 238 (2018) 576–585, https://doi.org/10.1016/j.apcatb.2018.07.065.

[36] M.Z. Memon, G. Ji, J. Li, M. Zhao, Na_2ZrO_3 as an effective bifunctional catalyst-sorbent during cellulose pyrolysis, Ind. Eng. Chem. Res. 56 (2017) 3223–3230, https://doi.org/10.1021/acs.iecr.7b00309.

[37] L.M. Palacios-Romero, H. Pfeiffer, Lithium cuprate (Li_2CuO_2): a new possible ceramic material for CO_2 chemisorption, Chem. Lett. 37 (2008) 862–863, https://doi.org/10.1246/cl.2008.862.

[38] Y. Matsukura, T. Okumura, R. Kobayashi, K. Oh-ishi, Synthesis and CO_2 absorption properties of single-phase Li_2CuO_2 as a CO_2 Absorbent, Chem. Lett. 39 (2010) 966–967, https://doi.org/10.1246/cl.2010.966.

[39] P.S.S. Babu, P.D. Vaidya, Sorption-enhanced steam methane reforming over Ni/Al_2O_3/$KNaTiO_3$ bifunctional material, J. Indian Chem. Soc. 99 (2022), https://doi.org/10.1016/j.jics.2022.100430.

[40] A. Yañez-Aulestia, H. Pfeiffer, The role of nickel addition on the CO_2 chemisorption enhancement in Ni-containing Li_2CuO_2: analysis of the cyclability and different CO_2 partial pressure performance, Fuel 277 (2020), 118185, https://doi.org/10.1016/j.fuel.2020.118185.

[41] A. Yañez-Aulestia, M.A. Martínez-Cruz, H. Pfeiffer, Evaluation of Me-Li_2CuO_2 solid solutions (where Me = Ni, Fe, and Mn) during CO_2 and CO chemisorption, J. Phys. Chem. C 124 (2020) 16019–16031, https://doi.org/10.1021/acs.jpcc.0c04614.

[42] G. Jabotra, P.K. Yadav, S. Kumar, S. Sharma, CO_2/CO methanation over Ru and Ni supported γ-Al_2O_3: a study on the effect of the stoichiometry of reactant gases, Mol. Catal. (2023) 547, https://doi.org/10.1016/j.mcat.2023.113365.

[43] S. Yoo, S. Park, J.H. Song, D.H. Kim, Hydrogen production by the steam reforming of ethanol over K-promoted Co/Al_2O_3–CaO xerogel catalysts, molecular catalysis, Mol. Catal. (2020) 491, https://doi.org/10.1016/j.mcat.2020.110980.

[44] G. Svehla, Vogel's Textbook of Macro and Semimicro Qualitative Inorganic Analysis, Longman Inc. New York, 1979, pp. 215–289. fifth ed.

[45] Y. Xu, B. Lu, C. Luo, J. Chen, Z. Zhang, L. Zhang, Sorption enhanced steam reforming of ethanol over Ni-based catalyst coupling with high-performance CaO pellets, Chem. Eng. J. 406 (2021), https://doi.org/10.1016/j.cej.2020.126903.

[46] M. Cortazar, S. Sun, C. Wu, L. Santamaria, L. Olazar, E. Fernandez, M. Artetxe, G. Lopez, M. Olazar, Sorption enhanced ethanol steam reforming on a bifunctional Ni/CaO catalyst for H_2 production, J. Environ. Chem. Eng. 9 (2021), https://doi.org/10.1016/j.jece.2021.106725.

[47] E.M. Mendoza-Núñez, J.C. Fierro-Gonzalez, T.A. Zepeda, A. Solis-Garcia, Effect of platinum addition on the reaction mechanism of the CO_2 methanation catalyzed by ZrO_2-supported Rh, Mol. Catal. (2022) 533, https://doi.org/10.1016/j.mcat.2022.112801.

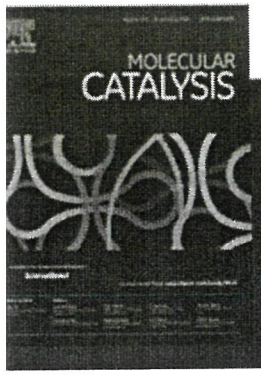

Molecular Catalysis

6.9
CiteScore

4.6
Impact Factor

The Impact Factor measures the average number of citations received in a particular year by papers published in the journal during the two preceding years. 2022 Journal Citation Reports (Clarivate Analytics, 2023)

Volume 553

15 January 2024